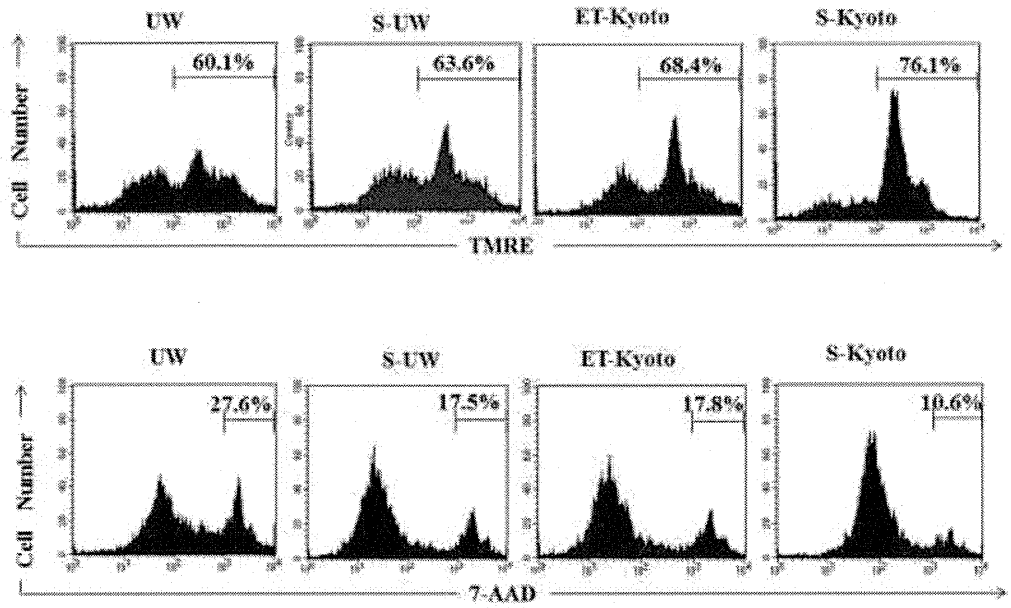

Figure 5

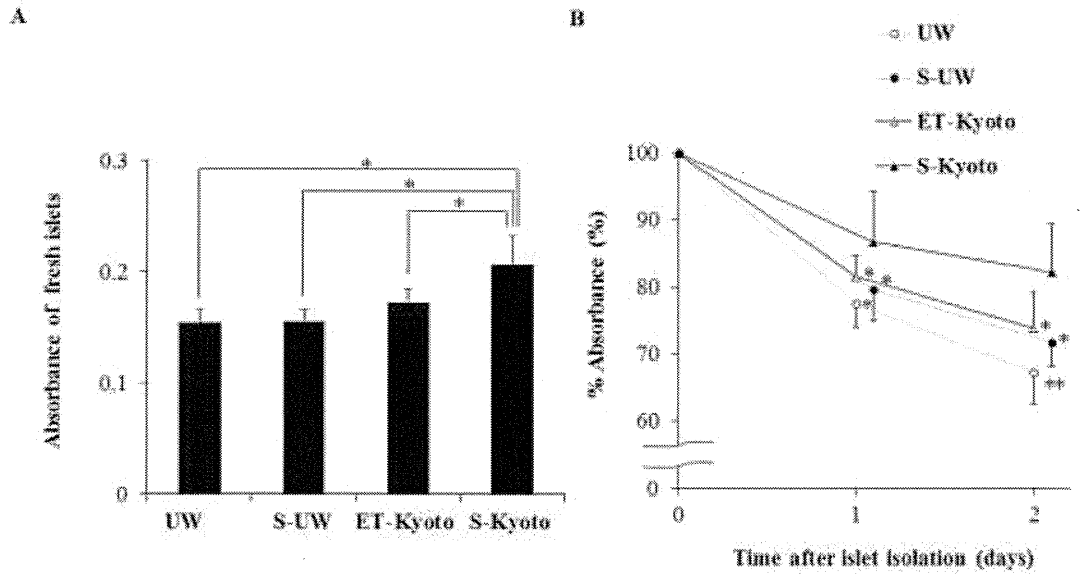

Figure 6

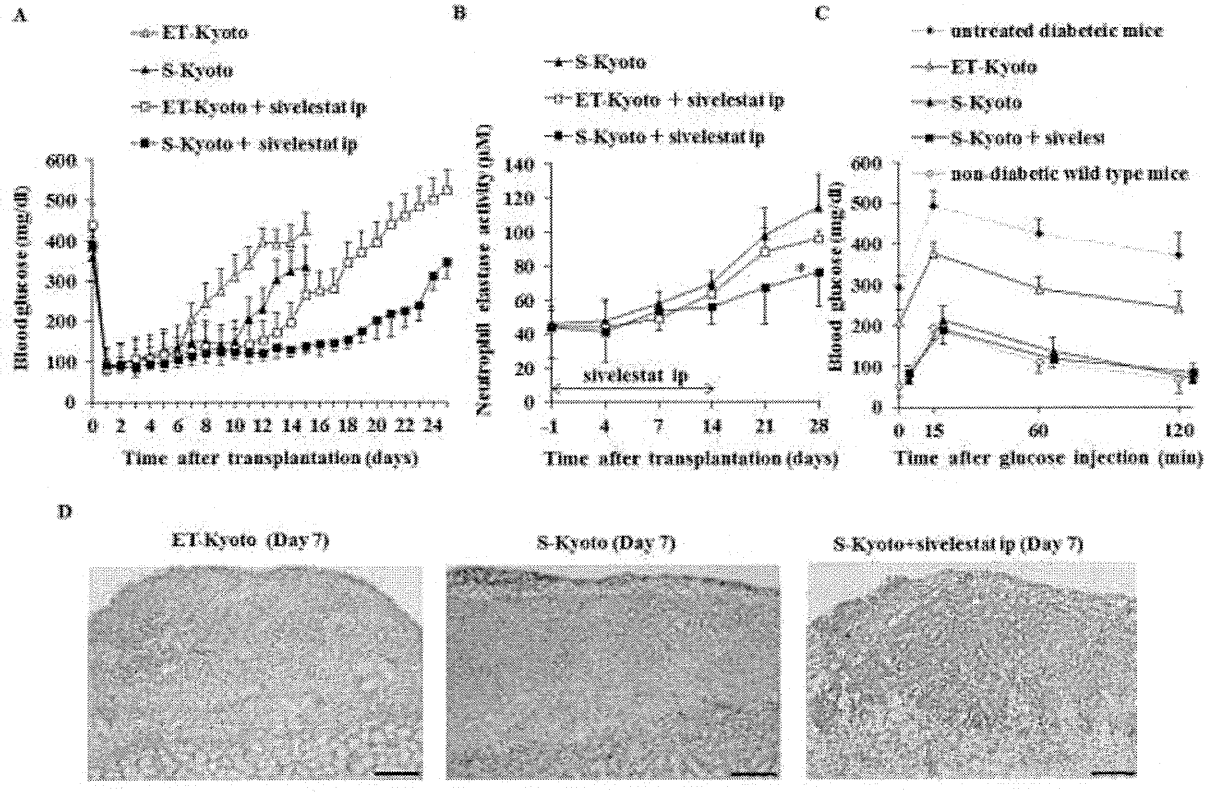

Figure 7

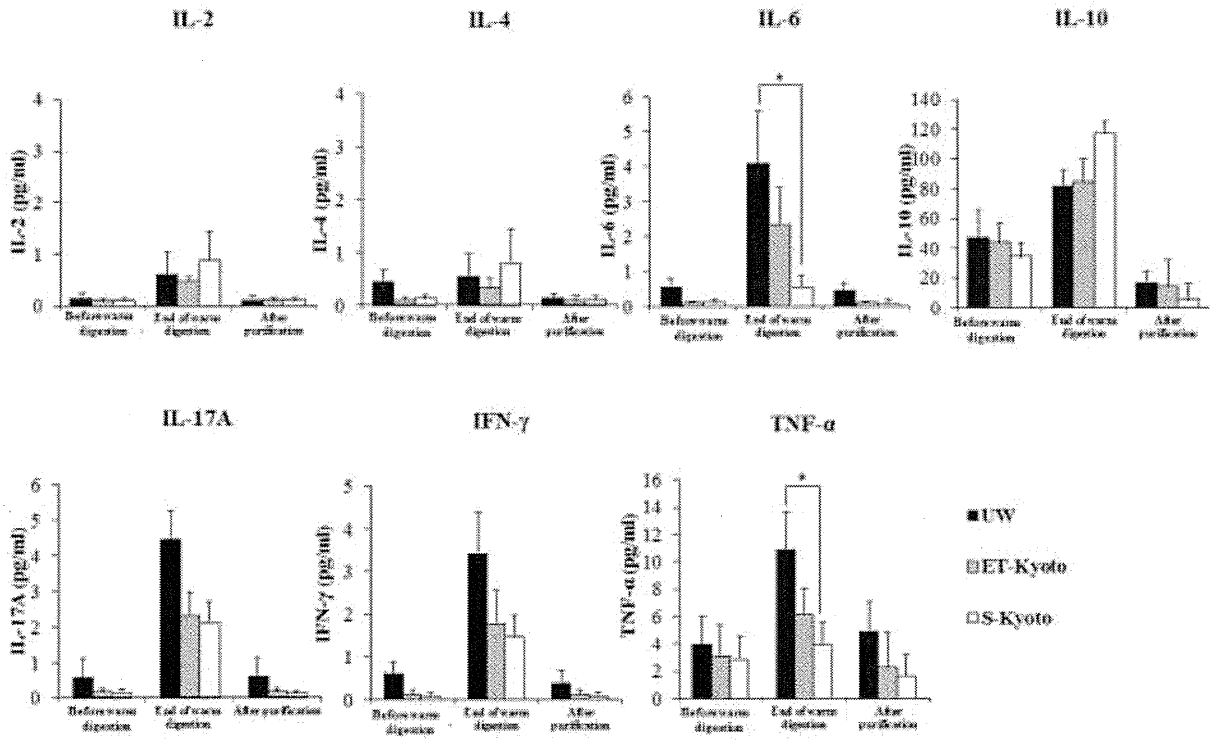

Figure 8

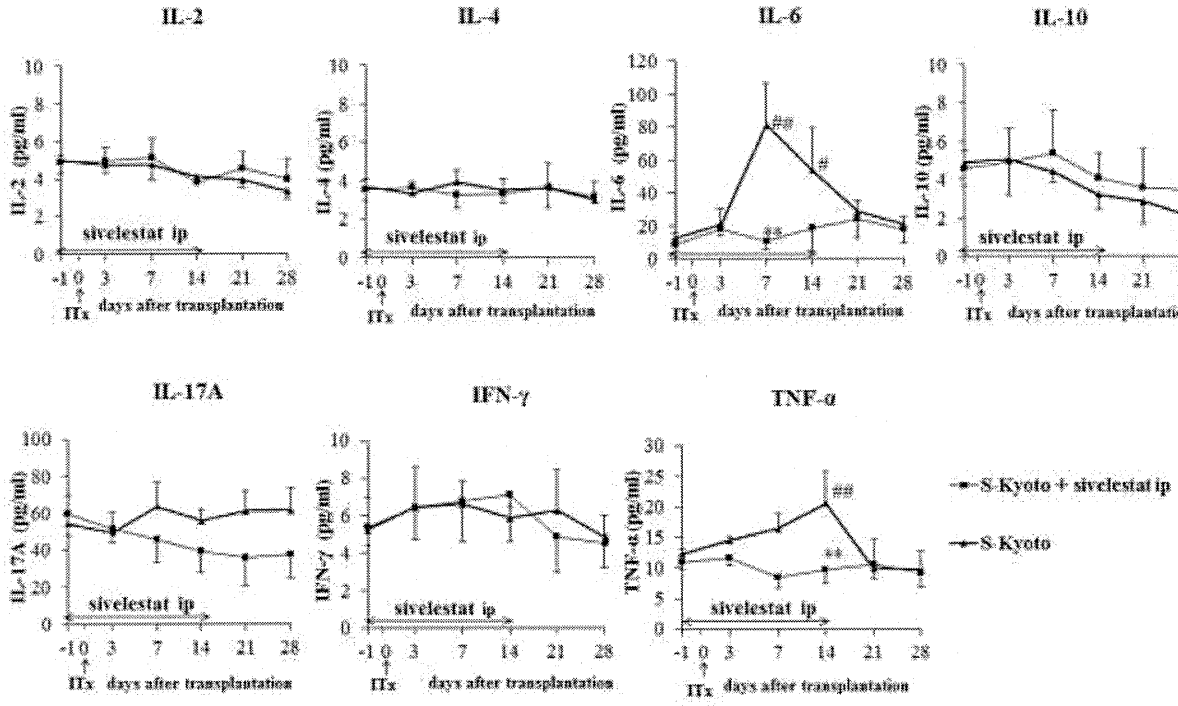

Figure 9

Surg Today (2012) 42:181–184
DOI 10.1007/s00595-011-0106-4

CASE REPORT

Tissue engineered myoblast sheets improved cardiac function sufficiently to discontinue LVAS in a patient with DCM: report of a case

Yoshiki Sawa · Shigeru Miyagawa · Taichi Sakaguchi · Tomoyuki Fujita · Akifumi Matsuyama · Atsuhiro Saito · Tatsuya Shimizu · Teruo Okano

Received: 15 August 2010 / Accepted: 31 January 2011 / Published online: 27 December 2011

Abstract Dilated cardiomyopathy (DCM) is a heart muscle disease characterized by progressive heart failure, and is a leading cause of mortality and morbidity. Recently, cellular therapy for end-stage heart failure has been emerging. We herein report a 56-year-old male who received a transplant of autologous myoblast sheets manufactured in temperature-responsive culture dishes. His clinical condition improved markedly, leaving him without any arrhythmia and able to discontinue using a left ventricular assist system and avoid cardiac transplantation. These findings suggest that cellular therapy using myoblast sheets is a promising new strategy for treating patients with end-stage DCM. This method might be an effective alternative to heart transplantation in the near future.

Keywords Cell · DCM · Tissue engineering · LVAD

Introduction

We herein report a patient with dilated cardiomyopathy (DCM) who received a transplant of autologous myoblast sheets that were manufactured using temperature-responsive culture dishes. After the treatment, the patient was able to discontinue using a left ventricular assist system (LVAS). This novel method represents a promising strategy for clinical myocardial cellular therapy in patients with end-stage DCM.

Y. Sawa (✉) · S. Miyagawa · T. Sakaguchi · T. Fujita
Department of Cardiovascular Surgery, Osaka University Graduate School of Medicine, 2-2 Yamada-oka, Suita, Osaka 565-0871, Japan
e-mail: sawa@surg1.med.osaka-u.ac.jp

A. Matsuyama · A. Saito
Medical Center of Translational Research, Osaka University Graduate School of Medicine, Suita, Japan

T. Shimizu · T. Okano
Tokyo Women's Medical University Institute of Advanced Biomedical Engineering and Science, Tokyo, Japan

Case report

A 56-year-old male, who was suffering from idiopathic DCM (Fig. 2h), was referred to Osaka University Hospital under intra-aortic balloon pump (IABP) support, oxygenation with a respirator, portable cardiopulmonary bypass, and continuous venovenous hemodiafiltration (CVVHD). Upon admission, he received an implantation of an extracorporeal pneumatic LVAS (Toyobo, Tokyo, Japan) and RVAS-ECMO using a centrifugal pump. At 7 and 8 months after admission, he was examined to determine whether the LVAS could be discontinued. Before LVAD implantation, his ejection fraction (EF) was 11%. After LVAD implantation, an off-pump test revealed that his EF was 20%. Therefore, LV unloading by LVAD implantation had improved the cardiac function, but the results did not meet the criteria for LVAS explantation as described by Dandel et al. [1], and we judged that it was inadvisable to explant the LVAS at that time.

Myoblast cell sheet transplantation for this patient was approved by the Ethical Committee and Internal Review Board of Osaka University. Upon granting his informed consent, the patients had an approximately 10-g piece of skeletal muscle excised from his medial vastus muscle under general anesthesia. The autologous myoblasts derived from this muscle were cultured according to published procedures [2], grown to 3×10^8 cells (more than

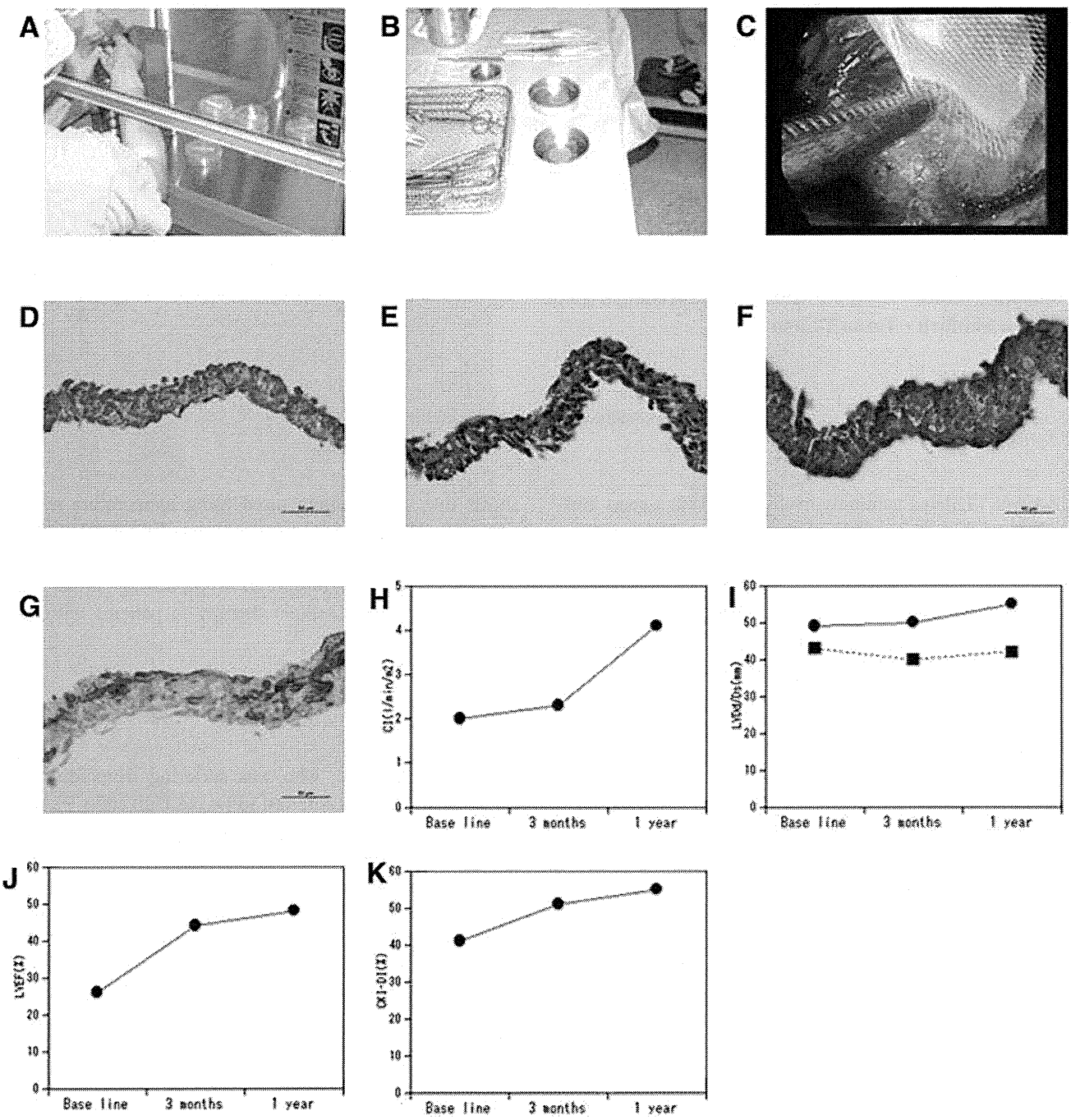

Fig. 1 The histology of the myoblast sheet and the changes in hemodynamic variables from baseline (before myoblast sheet implantation), and at 3 months and 1 year follow-up examinations. Hemodynamic variables at baseline and at the 3-month follow-up were obtained at the examination for LVAS removal. **a**, **b** Preparation of myoblast sheets in the operating room. **c** Implantation of a myoblast sheet via a left lateral thoracotomy. **d** HE staining of a myoblast sheet; the myoblast sheet included many cells, and its thickness was about 50 μm. **e** Masson-Trichrome staining; the myoblast sheet consisted of cells and extracellular matrix. **f** Desmin staining; nearly all of the cells in the myoblast sheets were Desmin positive. **g** Alpha-myosin heavy chain staining; some cells in the myoblast sheets were Alpha-myosin heavy chain positive. **h** Cardiac index. **i** LVDd (*solid line*) and LVDs (*dotted line*). **j** LV ejection fraction. **k** Color kinesis diastolic indices (CK-DI)

90% purity by FACS analysis with CD56) for 3 weeks, and seeded onto temperature-responsive culture dishes. They formed cell sheets after 48 h, as previously reported. The diameter of the myoblast sheet was about 4 cm and was round in shape. We implanted 4-layered myoblast sheets on one site and a total of 20 myoblast sheets (on five sites) to

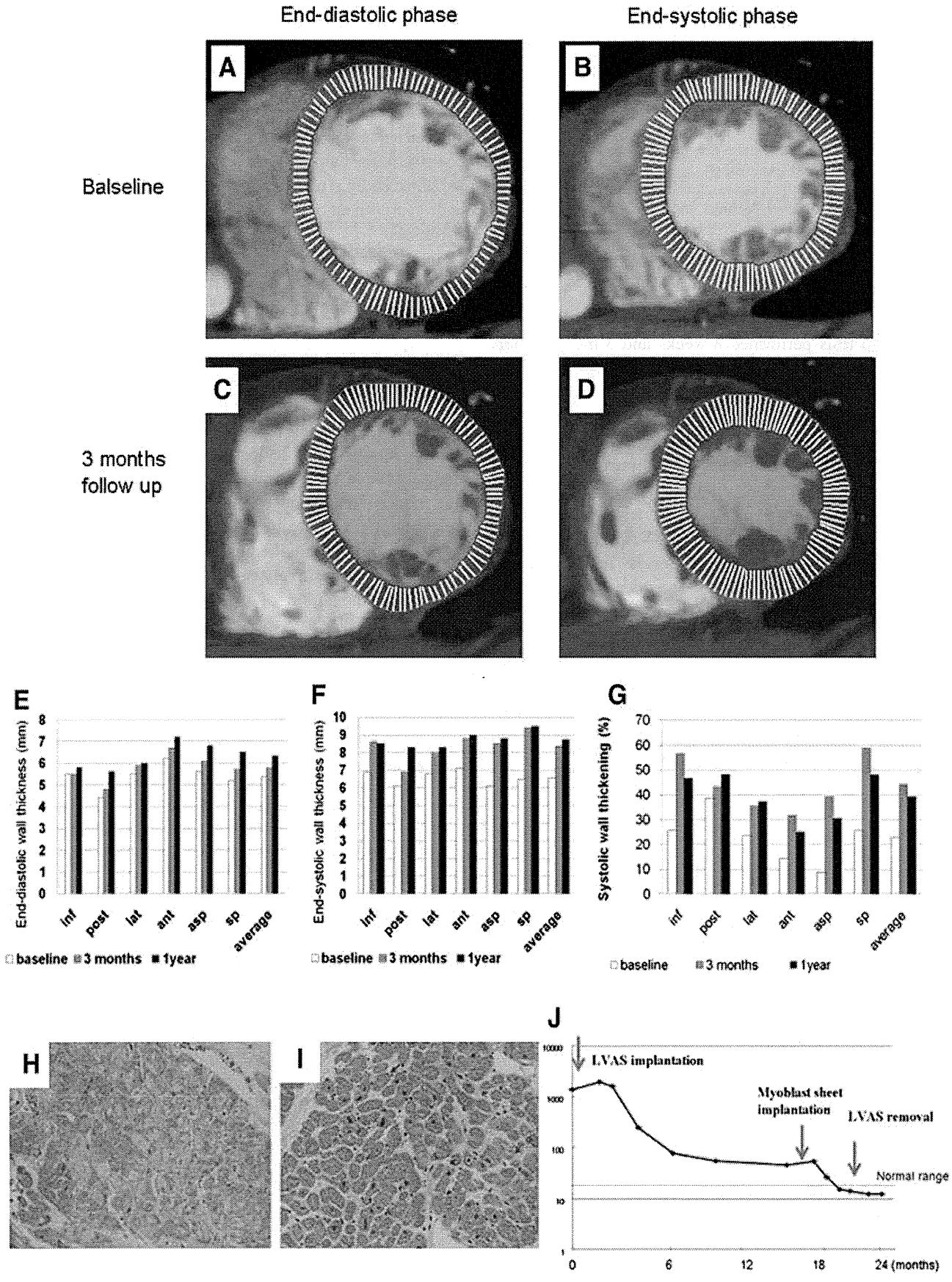
End-diastolic phase
End-systolic phase
Balseline
3 months follow up
A
B
C
D
E
End-diastolic wall thickness (mm)
inf post lat ant asp sp average
baseline 3 months 1year
F
End-systolic wall thickness (mm)
inf post lat ant asp sp average
baseline 3 months 1year
G
Systolic wall thickening (%)
inf post lat ant asp sp average
baseline 3 months 1year
H
I
J
LVAS implantation
Myoblast sheet implantation
LVAS removal
Normal range
0 6 12 18 24 (months)

◀ **Fig. 2** Changes from baseline in the regional wall thickness of the LV at 3 months and 1 year follow-up. **a–d** Images of the end-diastolic (**a**, **c**) and end-systolic (**b**, **d**) phase at baseline (**a**, **b**) and at the 3-month follow-up (**c**, **d**). The calculated wall thickness of each segment is shown in **e** (end-diastolic phase) and **f** (end-systolic phase), and the percent wall thickening is shown in **g**. The surgical specimens were obtained from the LV apical core removed at the time of LVAS implantation (**h**), and the needle biopsy of the LV anterior wall at the time of LVAS removal (**i**). Specimens were stained with hematoxylin–eosin (HE) by a conventional technique. **j** After LVAS implantation, the BNP level declined and reached a plateau. After myoblast sheet implantation, the BNP levels declined again to within the normal range

the anterior to lateral surface of the dilated heart through a left lateral thoracotomy.

Off-pump tests performed 8 weeks and 3 months after transplantation revealed that the ejection fraction was improved from 26 to 46%, and the LVDd from 49 to 53 mm (Fig. 1b, c). These data met the criteria for the explantation of LVAS, which was subsequently performed. Comparison of the wall motion pre- and post-treatment by color kinesis revealed improvement first on the anterior and lateral surfaces and then, in the longer term, on the other surface (Fig. 2). After starting the LVAS, the patient's brain natriuretic peptide (BNP) levels had gradually declined and reached a plateau. Subsequently, after myoblast sheet implantation, the BNP levels declined again and reached the normal range (Fig. 2j). The patient was discharged 7 months after myoblast sheet transplantation and has been an out-patient for more than 1 year. Regarding his clinical course after both cell sheet transplantation and LVAD removal, a Holter cardiogram demonstrated that no life-threatening arrhythmia had occurred.

Discussion

Menasche et al. [3] recently concluded that myoblast injections combined with coronary surgery in patients with depressed LV function fail to improve echocardiographic heart function. The proportion of injected cells surviving to engraft the infarcted myocardium is very low, owing to injected cells leaking from the intended region and being carried to other organs [4]. This loss of cells has therefore limited the applicability of this form of myoblast cell therapy [3].

To overcome these problems, we have developed a novel cell delivery system [5] that uses myoblast cell sheets, and performed animal investigations to guide clinical trials [4]. Using temperature-responsive tissue engineering techniques, we were able to transplant a larger numbers of cells, with greater viability, than by myoblast injection, and such cell sheets engrafted to the failed myocardium in rats led to improvements in cardiac function and tissue remodeling [4]. Although the myoblasts cannot transdifferentiate to cardiomyocytes, the myoblast sheets produce cytokines such as hepatocyte growth factor (HGF), which may have a positive impact on c-Met-expressing damaged myocardium [4], thus leading to the attenuation of fibrosis, angiogenesis, and recruitment of stem cells induced by paracrine cytokines.

In cellular therapy for cardiac disease, arrhythmogenesis is expected to occur in animal models and in clinical trials [3]; however, life-threatening arrhythmias have not been clinically observed after autologous cell sheet transplantation. In the case of injection, scarring of the myocardium is likely, and such scars can induce arrhythmias. Using our cell delivery technique, there may be less risk for inducing arrhythmia. Myoblasts have a weak electrical potential, and it may thus be possible for them to induce arrhythmia if they survive in the myocardium. However, cell sheets may not induce arrhythmia owing to their attachment to the epicardium.

In conclusion, autologous myoblast cell sheet transplantation may positively contribute to the improvement of the clinical condition of patients with DCM, allow the discontinuation of LVAS, and avoid heart transplantation. This therapy therefore shows promise for clinical myocardial regeneration in patients with end-stage DCM.

References

1. Dandel M, Weng Y, Siniawski H, Potapov E, Lehmkuhl HB, Hetzer R. Long-term results in patients with idiopathic dilated cardiomyopathy after weaning from left ventricular assist devices. Circulation. 2005;112:I37–45.
2. Hata H, Matsumiya G, Miyagawa S, et al. Grafted skeletal myoblast sheets attenuate myocardial remodeling in pacing-induced canine heart failure model. J Thorac Cardiovasc Surg. 2006;132:918–24.
3. Menasche P, Alfieri O, Janssens S, et al. The myoblast autologous grafting in ischemic cardiomyopathy (MAGIC) trial: first randomized placebo-controlled study of myoblast transplantation. Circulation. 2008;117:1189–200.
4. Memon IA, Sawa Y, Fukushima N, et al. Repair of impaired myocardium by means of implantation of engineered autologous myoblast sheets. J Thorac Cardiovasc Surg. 2005;130:1333–41.
5. Miyagawa S, Sawa Y, Sakakida S, et al. Tissue cardiomyoplasty using bioengineered contractile cardiomyocyte sheets to repair damaged myocardium: their integration with recipient myocardium. Transplantation. 2005;80:1586–95.

Journal of Bioscience and Bioengineering
VOL. 113 No. 1, 128–131, 2012

ELSEVIER

www.elsevier.com/locate/jbiosc

TECHNICAL NOTE

Evaluation of vertical cell fluidity in a multilayered sheet of skeletal myoblasts

Masahiro Kino-oka,[1,*] Trung Xuan Ngo,[2] Eiji Nagamori,[1] Yasunori Takezawa,[2] Yasuki Miyake,[2] Yoshiki Sawa,[3] Atsuhiro Saito,[3] Tatsuya Shimizu,[4] Teruo Okano,[4] and Masahito Taya[2]

Department of Biotechnology, Graduate School of Engineering, Osaka University, 2-1 Yamada-oka, Suita, Osaka 565-0871, Japan,[1] Division of Chemical Engineering, Graduate School of Engineering Science, Osaka University, 1-3 Machikaneyama-cho, Toyonaka, Osaka 560-8531, Japan,[2] Department of Surgery, Division of Cardiovascular Surgery, Graduate School of Medicine, Osaka University, 2-15 Yamada-oka, Suita, Osaka 565-0871, Japan,[3] and Institute of Advanced Biomedical Engineering and Science, Tokyo Women's Medical University, 8-1 Kawada-cho, Shinjuku-ku, Tokyo 162-8666, Japan[4]

Received 19 August 2011; accepted 5 September 2011
Available online 20 October 2011

The procedure for fabricating a multilayered cell sheet has been developed by combining multiple sheets using a thermo-responsive surface and stamp system. Confocal laser scanning microscopy revealed that the fluidity of a multilayered sheet of skeletal myoblasts could be estimated as vertical diffusivity and changed upon addition of dermal fibroblasts.

[**Key words:** Cell sheet; Skeletal myoblasts; Dermal fibroblasts; Cell migration; Sheet fluidity; Image processing]

Cell sheet engineering is emerging as an advanced technique for preparing scaffold-free 3-dimensional (3-D) tissue (1), not only for transplantation but also for *in vitro* research. A temperature-responsive poly-*N*-isopropylacrylamide (PIPAAm) grafted surface can be used to form a cell sheet without any enzymatic digestion, thereby which permits to retain an intact extracellular matrix (ECM) (1). Sasagawa et al. previously constructed a multilayered structure of skeletal muscle myoblast cells in which prevascular formation by endothelial migration was observed (2).

Cell migration in 3-D constructs plays an important role in physiological and pathological phenomena such as embryonic development, cell alignment, immune reaction, angiogenesis, and metastasis (3). Understanding the mechanisms of cell migration will be useful in the design of biomimetic structures and functional engineered tissues. Although the behaviors of cells on 2-D culture surfaces have been extensively investigated (4–7), spatial cell movement in 3-D tissues, especially with regard to vertical migration inside the tissue, has not been investigated due to the absence of methods to allow *in vitro* quantitative and reproducible measurements. In the present study, a five-layered skeletal myoblast sheet was fabricated as a 3-D model to evaluate vertical cell migration by confocal laser scanning microscopy and image processing.

Human skeletal muscle myoblasts (HSMMs; Lot. No. 4F1618; Lonza Walkersville Inc., Walkersville, MD, USA) and human dermal fibroblasts (HDFs; Lot. No. 6F4296; Lonza Walkersville Inc.) were used in the experiments. According to procedures described elsewhere (5, 8), the subcultures of HSMMs on laminin-coated surfaces were carried out at 37°C in an atmosphere of 5% CO_2 in Dulbecco's modified Eagle's medium (DMEM; Sigma-Aldrich, St. Louis, MO, USA) containing 10% fetal bovine serum (FBS; Invitrogen, Grand Island, NY, USA) and antibiotics (100 U/cm^3 penicillin G, 0.1 mg/cm^3 streptomycin, and 0.25 mg/cm^3 amphotericin B; Invitrogen).

As shown in Fig. 1A, starter cells harvested from the subcultures were stained using CellTracker Green™ and CellTracker Orange™ (Invitrogen) to exhibit fluorescently green and orange cells, respectively, according to commercially recommended protocol (5 μM for 15 min for live cell imaging). The stained cells were employed in the fabrication of the multilayered sheet according to newly developed procedures as follows. HSMMs were seeded at 2.3×10^5 cells/cm^2 in each well (diameter, 1.9 cm^2) of 24-well UpCell™ plates (CellSeed, Tokyo) with a temperature-responsive surface grafted with PIPAAm and incubated for 24 h at 37°C in 5% CO_2 to form the monolayer sheet. The medium depth was set to 2 mm throughout the experiments and HDFs were mixed into the sheet if needed. For stacking monolayer cell sheets to form the multilayered cell sheet, a manipulator was designed as shown in Fig. 1B composed of a stamp, its stand, and a mold to load the stamp with the gelatin gel. A solution of 7.4% gelatin was prepared by dissolving gelatin powder (G1890-100G; Sigma-Aldrich) in 5 mL Hank's balance salt solution (Sigma-Aldrich) and 100 μL of 1 N NaOH solution at 45°C for 30 min. The solution was then sterilized by filtration through a 0.22-μm filter (Millex-GS; Millipore Co., Billerica, MA, USA) and poured into the silicone molds under aseptic conditions. The stamps were put onto the molds on ice to gelation. Finally, the molds were gently removed and the stamps with the gelatin were ready to be used to stack the cell sheets. To harvest the monolayer sheet, the stamp with the gelatin gel was overlaid on the monolayer sheet in a well at 37°C and the temperature was shifted to 20°C (Fig. 1A). After 30 min, the stamp was lifted together with the monolayer sheet from the bottom surface of the well. The steps were

* Corresponding author. Tel.: +81 6 6879 7444; fax: +81 6 6879 4246.
E-mail address: kino-oka@bio.eng.osaka-u.ac.jp (M. Kino-oka).

1389-1723/$ - see front matter © 2011, The Society for Biotechnology, Japan. All rights reserved.
doi:10.1016/j.jbiosc.2011.09.001

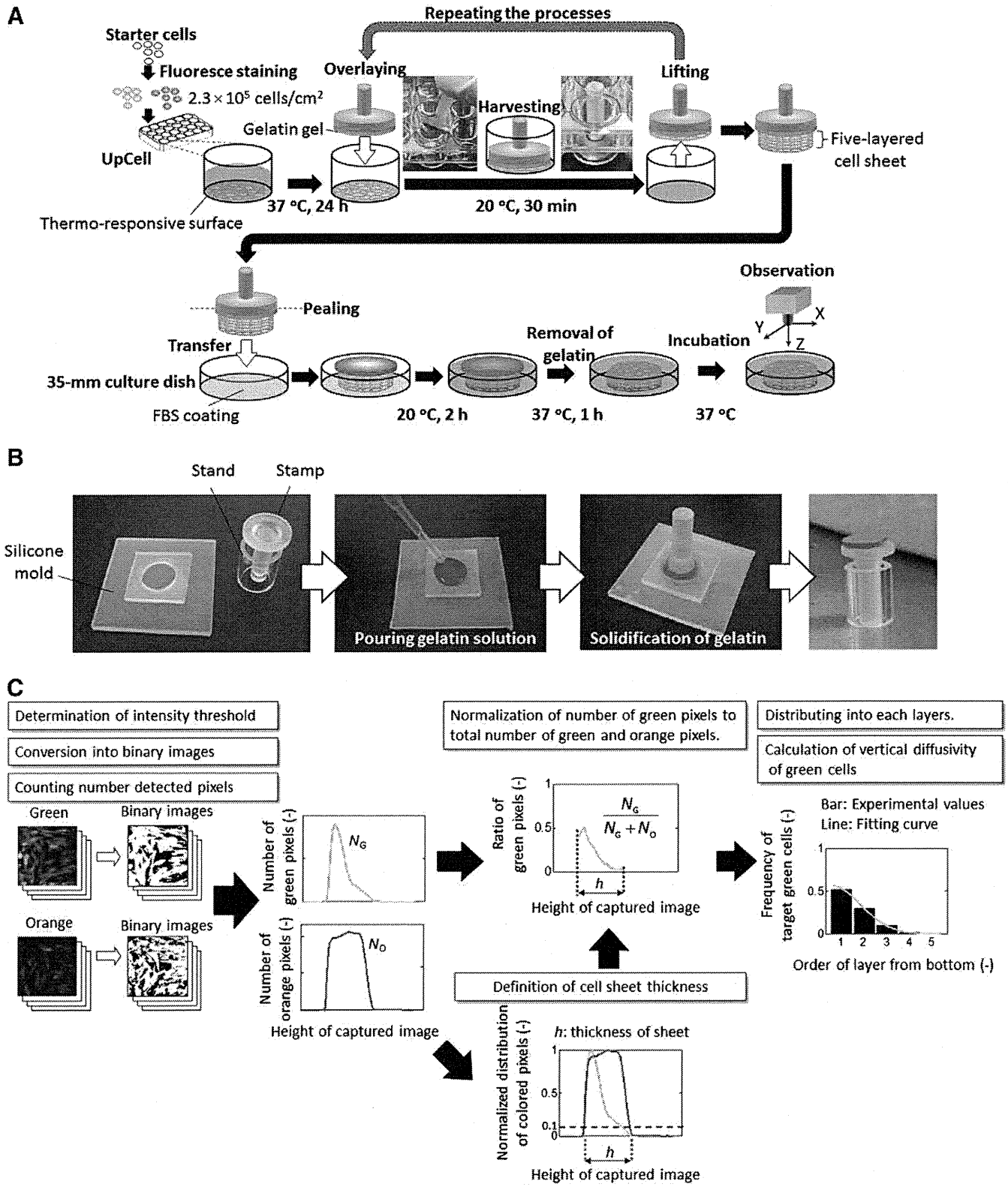

FIG. 1. Schematic diagrams showing the five-layered cell sheet fabrication and quantitative diffusivity analysis. (A) Fabrication of the five-layered cell sheet. (B) Preparation of the manipulator used to harvest the cell sheet. (C) Image processing system calculating the spatial distribution and diffusivity of the green target cells.

then repeated for the sequential harvests of monolayer sheets to form the multilayer structure on the stamp. The multilayered sheet with the gelatin was separated from the stamp and placed on a 35-mm culture dish (ibidi GmbH, Martinsried, Germany) that was precoated with 0.2 mL/cm^2 FBS for 24 h for the facilitation of the sheet attachment to the surface, and the dish was incubated for 2 h at 20°C in 5% CO_2 without the addition of medium. To remove gelatin, the medium (0.4 mL/cm^2) was added, and the temperature was

shifted to 37°C for 1 h to melt the gelatin and the medium was changed with a fresh one. In the present study, the fabricated culture system of a five-layered sheet was used to analyze sheet behaviors.

As a typical culture system, the five-layered sheet consisting of basal layers (green) and other layers (orange) stained by CellTracker Green™ and CellTracker Orange™, respectively, was prepared for the observation of tempo-spatial cell distribution using confocal laser scanning microscopes (FV10i for time lapse and FV-300 for spatial distribution; Olympus, Tokyo) with 60× objective lens. To determine the spatial distribution of the target cells, the green and orange cells in each layer at 0 and 48 h of incubation were observed and quantitatively analyzed using image processing (Fig. 1C). The five-layered sheet was washed twice with phosphate buffered saline (PBS) and then fixed with 4% paraformaldehyde in PBS (Wako Pure Chemical Industries, Osaka) overnight. After washing with PBS, at least eight random positions of each sample were scanned at a 0.6-μm interval to yield slice images for vertical direction determination. After intensity threshold values were identified, 8-bit images (256×256 pixels) of both colors in each slice were converted into binary images, leading to the distinction between colored and non colored pixels. Here the colored pixels which were derived from green and orange fluorescent original images denoted the green and orange pixels, respectively. The number of colored pixels in each slice was counted. The green and orange pixels in each slice were normalized using the maximum green and orange pixel values, respectively, found in all of the slice images. The slice possessing more than 10 % of the colored pixels was regarded to exist inside cell sheet, from which the vertical positions at top and bottom of the five-layered sheet, and the sheet thickness, h, were determined. The ratio of green pixels to sum of green and orange pixels in each slice was normalized to determine the distribution of green pixels by dividing into 5 layers. Here, the normalized distribution of green pixels was assumed to be equivalent to the green cell distribution in the sheet, recorded by the frequency of green cells, f_G, in each layer.

Time-lapse observation was conducted of the five-layered sheet (Supplementary Movie S1). During the early incubation period, the green cells were observed in the bottom of the sheet, and the active cellular migration occurred in the horizontal and vertical directions anywhere in the sheet, revealing the sheet fluidity. The green cells then migrated toward the upper layers as time elapsed. To understand the extent of the sheet fluidity, the vertical distribution of green cells was estimated. Figure 2 shows the histograms of f_G at 0 and 48 h. The f_G values in the first and second layers from the bottom surface were estimated to be $f_G = 0.82$ and 0.17, respectively, and the sheet at 48 h had a broad distribution of f_G, being $f_G = 0.37$ in the first layer. In addition, the f_G decreased gradually along the layers from bottom to top, suggesting the analogy of vertical migration to molecular diffusion. To quantitatively analyze vertical sheet fluidity, the diffusivity, D, was determined based on Fick's second law, $\frac{\partial f_G}{\partial t} = D\frac{\partial^2 f_G}{\partial h^2}$, in which f_G, t, and h represent the green cell frequency, incubation time, and sheet thickness, respectively. The Crank–Nicolson finite difference method and least squares method were applied to calculate the diffusivity using a custom-made software programmed by LabVIEW (National Instruments, Austin, TX, USA). The initial condition was that the total ratio of green cells in the five layers was normalized to unity. The free boundary condition, $\frac{df_G}{dh} = 0$, is set at both the bottom and the top of the five-layered sheet. In a practical aspect, the f_G distribution data at 0 and 48 h were applied to calculate the apparent vertical diffusivity of green cells, $\bar{D}_o$, being $\bar{D}_o = 0.74\ \mu m^2/h$ (Table 1).

To investigate sheet fluidity variation, we incubated five-layered sheets added with HDFs comprising 25% and 50% of the cell counts (conditions B and C, respectively). As shown in Table 1, the $\bar{D}_o$ increased at 25% addition (condition B) compared to that without any HDF addition (condition A), although the significance level was not sufficient ($p<0.06$). In addition, 50% addition (condition C) caused a decrease in $\bar{D}_o$ compared to that at 25% addition ($p<0.05$). For further understanding of the role of HDFs addition, we established the five-layered sheet system composed of HSMMs or HDFs in basal layer stained by CellTracker Green™ and the rest of cells stained by CellTracker Orange™, and estimated the diffusivity of basal HSMMs or HDFs, $\bar{D}_M$ or $\bar{D}_F$, respectively (Table 1). At 25% addition, $\bar{D}_F$ was estimated to be $2.40\ \mu m^2/h$, being 4 times larger than $\bar{D}_M$. At 50% addition, $\bar{D}_F$ decreased to $0.80\ \mu m^2/h$, although $\bar{D}_M$ stayed constant, suggesting that $\bar{D}_o$ depended on HDF migration in the sheet.

An independent experiment showed that the migration rate of single HDF is 1.5 times higher than that of single HSMMs in culture using a conventional T-flask (data not shown). Pittet et al. reported that HDFs exhibited strong OB-cadherin connection in high-density culture (9). These results suggest that HDF active migration physically facilitated the overall fluidity in the sheet at lower HDF addition levels. It is most likely that higher HDF addition induced strong HDF intracellular binding in the sheet, and this strong interaction with lower HDF migration rates resulted in the decline of overall sheet fluidity.

The inner structural fluidity of cells in 3-D constructs has been reported in cultured neurospheres (10) and embryoid bodies (11). In static suspension cultures of mouse neural stem cells, active migration of single cells caused aggregate formation through intercellular coalescence, and culture prolongation led to cell division in the aggregates as well as accidental coalescence between independent aggregates that formed large spheres in which the location of distribution of differentiated neurons and glia was observed (12). Further observation revealed that the large sphere was caused by spontaneous active migration in aggregates through the live-cell imaging technique. In addition, Duguay et al. (13) reported that aggregation using a mixture of E-cad-expressing E8a cell line and P-cad-expressing LP1 cell line caused spatial habitant isolation of 3-D spheres via active cell migration and intercellular binding affinity, leading to autonomous double-layer spheres by different cell types. These results mean the importance of cell migration in 3-D constructs

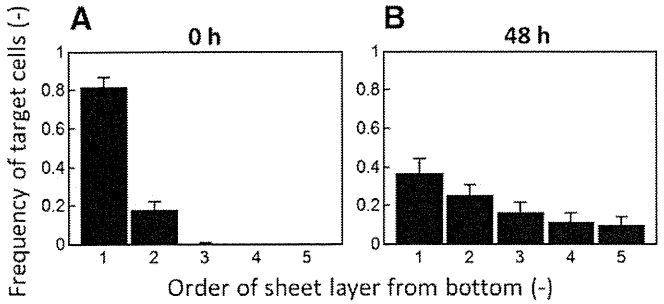

FIG. 2. Spatial distributions of the green target cells inside the cell sheet at 0 (A) and 48 h (B). Bars show the standard deviation (SD) ($n=3$).

TABLE 1. Diffusivities of different target cells from the basal layer in the five-layered cell sheet at different cellular balance conditions.

Condition	HSMMs (%)	HDFs (%)	Initial thickness of sheet, h (μm)	Diffusivity (μm²/h)		
				$\bar{D}_o$	$\bar{D}_M$	$\bar{D}_F$
A	100	0	33.0±5.4	0.74±0.23	–	–
B	75	25	36.4±5.4	1.57±0.50	0.57±0.14	2.40±0.49
C	50	50	37.7±5.0	0.69±0.12	0.54±0.26	0.80±0.36

$\bar{D}_o$, $\bar{D}_M$, and $\bar{D}_F$ are the diffusivities of whole cells, skeletal myoblasts, and dermal fibroblasts from the basal layer, respectively. HSMMs, human skeletal muscle myoblasts; HDFs, human dermal fibroblasts. All values were expressed as mean±SD ($n=3$).

affecting the fate of stem cells as well as spatial habitant isolation of differentiated cells. In the current study, HDF addition was found to affect sheet fluidity. Further experiments clarified the localization of HDFs in five-layered sheets (Oda, M. et al., Abstr., 10th Congress of the Japanese Society for Regenerative Medicine, p. 248, 2011). This finding suggested that the cell sheet fabricated from HMMs and HDFs exhibited the habitant isolation between them.

Many researchers have paid much attention to tissue mimicry by using cellular aggregates, which are considered minimized functional structures. The mimic constructs have broad potential use as transplants in regenerative medicine as well as structural material for elucidating the dynamic tissue development mechanism. From the standpoint of analytical techniques, observational convenience of 3-D constructs is a critical requirement because cellular behaviors such as migration, division, and communication affect the common mechanisms of tissue development.

In conventional studies, most of the techniques for fabricating cell aggregates led to spherically shaped constructs through spontaneous formation by cellular coagulation. In contrast, the current system applied the plate shape of the multilayered sheet using artificially designed formation by the assembly of monolayer sheets because the mimic system using the plate-shaped aggregate has the observational advantage in the 3-D construct. The plate-shaped aggregates can be fabricated in various ways using cell sheet engineering technique with thermo-responsive polymer grafted surface (1), biodegradable peptide grafted surface (14) or collagenase degradable atelocollagen film (15), magnetic-force based tissue engineering technique (16), layer-by-layer assembly technique with ECM coating cells (17), compressed collagen sheet (18), vitrified collagen film "vitrigel" (19), and bioprinting method (20).

Our system that uses multilayered sheet containing stained target cells in the basal layer and confocal laser scanning microscopy realizes clear observation of target cell behaviors in the vertical direction, enabling monodimensional analysis of vertical cell distribution inside the sheet. The reduced spatial dimension makes easy to analyze cell migration, compared to the full 3-D analysis required of spherically shaped aggregates. Thus, the system developed in the present study can be a powerful tool for elucidating dynamic phenomena in 3-D constructs.

Supplementary data to this article can be found online at doi:10.1016/j.jbiosc.2011.09.001.

This study was supported by the New Energy and Industrial Technology Development Organization (NEDO) of Japan, and the Japan Society for the Promotion of Science (JSPS) through the "Funding Program for World-Leading Innovative R&D on Science and Technology (FIRST Program)," initiated by the Council for Science and Technology Policy (CSTP).

References

1. **Yang, J., Yamato, M., Kohno, C., Nishimoto, A., Sekine, H., Fukai, F., and Okano, T.:** Cell sheet engineering: recreating tissues without biodegradable scaffolds, Biomaterials, **26**, 6415–6422 (2005).
2. **Sasagawa, T., Shimizu, T., Sekiya, S., Haraguchi, Y., Yamato, M., Sawa, Y., and Okano, T.:** Design of prevascularized three-dimensional cell-dense tissues using a cell sheet stacking manipulation technology, Biomaterials, **31**, 1646–1654 (2010).
3. **Horwitz, R. and Webb, D.:** Cell migration, Curr. Biol., **13**, R756–R759 (2003).
4. **Louis, M., Zanou, N., Van, S. M., and Gailly, P.:** TRPC1 regulates skeletal myoblast migration and differentiation, J. Cell Sci., **121**, 3951–3959 (2008).
5. **Chowdhury, S. R., Muneyuki, Y., Takezawa, Y., Kino-oka, M., Saito, A., Sawa, Y., and Taya, M.:** Synergic stimulation of laminin and epidermal growth factor facilitates the myoblast growth through promoting migration, J. Biosci. Bioeng., **108**, 174–177 (2009).
6. **Wang, W., Pan, H. Y., Murray, K., Jefferson, B. S., and Li, Y.:** Matrix metalloproteinase-1 promotes muscle cell migration and differentiation, Am. J. Pathol., **174**, 541–549 (2009).
7. **Bondesen, B. A., Jones, K. A., Glasgow, W. C., and Pavlath, G. K.:** Inhibition of myoblast migration by prostacyclin is associated with enhanced cell fusion, FASEB J., **21**, 3338–3345 (2007).
8. **Chowdhury, S. R., Muneyuki, Y., Takezawa, Y., Kino-oka, M., Saito, A., Sawa, Y., and Taya, M.:** Growth and differentiation potentials in confluent state of culture of human skeletal muscle myoblasts, J. Biosci. Bioeng., **109**, 310–313 (2010).
9. **Pittet, P., Lee, K. M., Kulik, A. J., Meister, J. J., and Hinz, B.:** Fibrogenic fibroblasts increase intercellular adhesion strength by reinforcing individual OB-cadherin bonds, J. Cell Sci., **121**, 877–886 (2008).
10. **Singec, I., Knoth, R., Meyer, R. P., Maciaczyk, J., Volk, B., Nikkhah, G., Frotscher, M., and Snyder, E. Y.:** Defining the actual sensitivity and specificity of the neurosphere assay in stem cell biology, Nat. Methods, **3**, 801–806 (2006).
11. **Dang, S. M., Kyba, M., Perlingeiro, R., Daley, G. Q., and Zandstra, P. W.:** Efficiency of embryoid body formation and hematopoietic development from embryonic stem cells in different culture systems, Biotechnol. Bioeng., **78**, 442–453 (2002).
12. **Mori, H., Ninomiya, K., Kanemura, Y., Yamasaki, M., Kino-oka, M., and Taya, M.:** Image cytometry for analyzing regional distribution of cells inside human neurospheres, J. Biosci. Bioeng., **103**, 384–387 (2007).
13. **Duguay, D., Foty, R. A., and Steinberg, M. S.:** Cadherin-mediated cell adhesion and tissue segregation: qualitative and quantitative determinants, Dev. Biol., **253**, 309–323 (2003).
14. **Qiu, F., Chen, Y., Cheng, J., Wang, C., Xu, H., and Zhao, X.:** A simple method for cell sheet fabrication using mica surfaces grafted with peptide detergent A(6)K, Macromol. Biosci., **10**, 881–886 (2010).
15. **Nagai, N., Yunoki, S., Satoh, Y., Tajima, K., and Munekata, M.:** A method of cell-sheet preparation using collagenase digestion of salmon atelocollagen fibrillar gel, J. Biosci. Bioeng., **98**, 493–496 (2004).
16. **Ito, A., Shinkai, M., Honda, H., and Kobayashi, T.:** Medical application of functionalized magnetic nanoparticles, J. Biosci. Bioeng., **100**, 1–11 (2005).
17. **Matsusaki, M., Kadowaki, K., Nakahara, Y., and Akashi, M.:** Fabrication of cellular multilayers with nanometer-sized extracellular matrix films, Angew. Chem. Int. Ed., **46**, 4689–4692 (2007).
18. **Brown, R. A., Wiseman, M., Chuo, C. B., Cheema, U., and Nazhat, S. N.:** Ultrarapid engineering of biomimetic materials and tissues: fabrication of nano- and microstructures by plastic compression, Adv. Funct. Mater., **15**, 1762–1770 (2005).
19. **Takezawa, T., Ozaki, K., Nitani, A., Takabayashi, C., and Shimo-Oka, T.:** Collagen vitrigel: a novel scaffold that can facilitate a three-dimensional culture for reconstructing organoids, Cell Transplant., **13**, 463–473 (2004).
20. **Nakamura, M., Iwanaga, S., Henmi, C., Arai, K., and Nishiyama, Y.:** Biomatrices and biomaterials for future developments of bioprinting and biofabrication, Biofabrication, **2**, 014110 (2010).

THE JOURNAL OF BIOLOGICAL CHEMISTRY VOL. 287, NO. 13, pp. 10590–10601, March 23, 2012
Published in the U.S.A.

Role of Epithelial-Stem Cell Interactions during Dental Cell Differentiation*[S]

Received for publication, August 4, 2011, and in revised form, January 5, 2012 Published, JBC Papers in Press, February 1, 2012, DOI 10.1074/jbc.M111.285874

Makiko Arakaki[‡1], Masaki Ishikawa[§1], Takashi Nakamura[‡], Tsutomu Iwamoto[‡], Aya Yamada[‡], Emiko Fukumoto[‡], Masahiro Saito[¶], Keishi Otsu[‖], Hidemitsu Harada[‖], Yoshihiko Yamada[§], and Satoshi Fukumoto[‡2]

From the [‡]Division of Pediatric Dentistry, Department of Oral Health and Development Sciences, Tohoku University Graduate School of Dentistry, Sendai 980-8575, Japan, the [§]Laboratory of Cell and Developmental Biology, NIDCR, National Institutes of Health, Bethesda, Maryland 20892, the [¶]Faculty of Industrial Science and Technology, Tokyo University of Science, Chiba 278-8510, Japan, and the [‖]Department of Oral Anatomy II, Iwate Medical College School of Dentistry, Morioka 020-8505, Japan

Background: The role of dental epithelium in stem cell differentiation has not been clearly elucidated.
Results: SP cells differentiated into odontoblasts by epithelial BMP4, whereas iPS cells differentiated into ameloblasts when cultured with dental epithelium.
Conclusion: Stem cells can be induced to odontogenic cell fates when co-cultured with dental epithelium.
Significance: This is the first report to show induction of ameloblasts from iPS cells.

Epithelial-mesenchymal interactions regulate the growth and morphogenesis of ectodermal organs such as teeth. Dental pulp stem cells (DPSCs) are a part of dental mesenchyme, derived from the cranial neural crest, and differentiate into dentin forming odontoblasts. However, the interactions between DPSCs and epithelium have not been clearly elucidated. In this study, we established a mouse dental pulp stem cell line (SP) comprised of enriched side population cells that displayed a multipotent capacity to differentiate into odontogenic, osteogenic, adipogenic, and neurogenic cells. We also analyzed the interactions between SP cells and cells from the rat dental epithelial SF2 line. When cultured with SF2 cells, SP cells differentiated into odontoblasts that expressed dentin sialophosphoprotein. This differentiation was regulated by BMP2 and BMP4, and inhibited by the BMP antagonist Noggin. We also found that mouse iPS cells cultured with mitomycin C-treated SF2-24 cells displayed an epithelial cell-like morphology. Those cells expressed the epithelial cell markers p63 and cytokeratin-14, and the ameloblast markers ameloblastin and enamelin, whereas they did not express the endodermal cell marker Gata6 or mesodermal cell marker brachyury. This is the first report of differentiation of iPS cells into ameloblasts via interactions with dental epithelium. Co-culturing with dental epithelial cells appears to induce stem cell differentiation that favors an odontogenic cell fate, which may be a useful approach for tooth bioengineering strategies.

Tooth morphogenesis is characterized by reciprocal interactions between dental epithelium and mesenchymal cells derived from the cranial neural crest, which result in formation of the proper number and shapes of teeth. Multiple extracellular signaling molecules, including BMPs, FGFs, WNTs, and SHH, have been implicated in these interactions for tooth development (1). Epithelial cells then subsequently give rise to enamel-forming ameloblasts, while mesenchymal stem cells (MSCs)[3] form dentin-forming odontoblasts and dental pulp cells. Initial tooth development is also regulated by extracellular matrices (ECMs), such as basement membrane components that include laminin, collagen, fibronectin, and perlecan (2, 3). These matrices control proliferation, polarity, and attachment, and also determine tooth germ size and morphology. At later stages of tooth development, the basement membrane components disappear and odontogenic cells begin to secrete a variety of tooth-specific extracellular matrices that give rise to layers of enamel and dentin, produced by epithelial-derived ameloblasts and mesenchymal-derived odontoblasts, respectively. Ameloblastin (Ambn) is one of the enamel matrix proteins expressed by differentiating ameloblasts, and is essential for dental epithelial cell differentiation into ameloblasts and enamel formation (2, 4). Dentin sialophosphoprotein (DSPP) is a member of the SIBLING (Small Integrin-Binding Ligand *N*-linked Glycoprotein) family of extracellular matrix glycophosphoproteins, and is expressed by differentiating ameloblasts and odontoblasts (5). These extracellular matrices are important for the formation of enamel and dentin (2).

Stem cell research has identified and established several types of stem cells, including induced pluripotent stem (iPS) cells, which are generated from a variety of somatic cell types via introduction of transcription factors that mediate pluripo-

* This work was supported, in whole or in part, by the Intramural Research Program of the NIDCR, National Institutes of Health (to Y. Y.). This work was also supported by Grants-in-aid 20679006 (to S. F.), 21792054 (to A. Y.), 21792154 (to E. F.) from the Ministry of Education, Science, and Culture of Japan, and the NEXT program (LS010, to S. F.), and by grants from the Takeda Science Foundation.

[S] This article contains supplemental Figs. S1–S5 and Table S1.

[1] Both authors contributed equally to this work.

[2] To whom correspondence should be addressed: Division of Pediatric Dentistry, Department of Oral Health and Development Sciences, Tohoku University Graduate School of Dentistry, Sendai 980-8575, Japan. Fax: 81-22-717-8386; E-mail: fukumoto@dent.tohoku.ac.jp.

[3] The abbreviations used are: MSC, mesenchymal stem cell; mDP, mouse dental pulp; Ambn, Ameloblastin; DSPP, dentin sialophosphoprotein; iPS, induced pluripotent stem; DPSC, dental pulp stem cell; SP, side population; MP, majority population; ALP, alkaline phosphatase; MEF, mouse embryonic fibroblasts; MMC, mitomycin C.

tency (6). Direct reprogramming of somatic cells into iPS cells by forced expression of a small number of defined factors (*e.g.* Oct3/4, Sox2, Klf4, and c-Myc) has great potential for tissue-specific regenerative therapies. In addition, this process also avoids ethical issues surrounding the use of embryonic stem (ES) cells, as well as problems with rejection following implantation of non-autologous cells (7). A variety of cell types, including hematopoietic precursor cells (8, 9), endothelial cells, MSCs, neuronal cells (10), reproductive cells (11), and cardiomyocytes (12, 13), undergo *in vitro* differentiation. However previous studies of dental cell differentiation are not adequate to explain this process. Several dental stem cell populations have been identified in different parts of the tooth, including cells from the periodontal ligament that links the tooth root with the bone, tips of developing roots, and tissue (dental follicle) that surrounds an unerupted tooth. In addition, dental pulp stem cells (DPSCs) have been identified in the pulp of exfoliated deciduous teeth of both children and adults (14). These different cell types likely share a common lineage, being derived from neural crest cells, and all have generic MSC-like properties.

Transplantation of *in vitro* expanded DPSCs mixed with hydroxyapatite/tricalcium phosphate particles results in the formation of dental pulp and dentin-like tissue complexes in immunocompromised mice (15). Similar results have been observed with an MSC population obtained from human exfoliated deciduous teeth (SHED) (14). DPSCs also express the putative stem cell marker STRO-1 and perivascular cell marker CD146, while a proportion co-expresses smooth muscle actin and the pericyte-associated antigen 3G5 (16). These findings suggest that a population of DPSCs may reside in this perivascular niche within the pulp of adult teeth.

Side population (SP) cells were identified by flow cytometry analysis with a Hoechst 33342 efflux assay and found to have stem cell characteristics (17). SP cells are a small population that show low levels of Hoechst dye staining for the expression of Abcg2, an ATP-binding cassette transporter (18), which is strongly expressed in dental pulp in human adult and deciduous teeth (19). Dental pulp contains multipotent stem cells and is viewed as a potential source of iPS cells (14, 20, 21). In tooth germ development, undifferentiated neural crest-derived MSCs interact with dental epithelium and differentiate into dentin matrix-secreting odontoblasts. However, the interactions between stem cells and dental epithelium have not been clearly elucidated.

In this study, we established an SP cell line from mouse dental papilla. We then cultured these SP cells with rat dental epithelial cells to investigate epithelial-mesenchymal interactions. SP cells were induced to differentiate into DSPP expressing odontoblasts via the action of epithelial BMP4. Furthermore, mouse iPS cells differentiated into Ambn-expressing dental epithelium when cultured with dental epithelial cells. Thus, these undifferentiated stem cells can be induced to an odontogenic cell fate when co-cultured with dental epithelial cells. These findings may be useful for analysis of dental cell differentiation *in vitro* and for procurement of odontogenic cells for use in regenerative medicine.

EXPERIMENTAL PROCEDURES

Preparation of Mouse Dental Papilla Cells—Dental papilla tissues were isolated from incisors from newborn ICR mice by digesting with 0.1% collagenase D (Roche) and 2.5% trypsin for 30 min at 37 °C. Enzymatically digested tissues were minced into 2–4 mm pieces using micro-scissors and washed three times with Dulbecco's modified Eagle's medium (DMEM) (Invitrogen) containing 10% fetal bovine serum (FBS) (Invitrogen) and an antibiotic-antimycotic mixture (Invitrogen), then filtered through a cell strainer (40 μm) to eliminate clumps and debris. Mouse dental papilla (mDP) cells were cultured in 60-mm culture dishes and immortalized by expression of a mutant human papilloma virus type 16 E6 gene lacking the PDZ-domain-binding motif (22). mDP cells were maintained with DMEM supplemented with 10% FBS and an antibiotic-antimycotic mixture at 37 °C in a humidified atmosphere containing 5% CO_2.

Generation of Dental Epithelial Cell Line SF2-24 and Cell Culture—Rat dental epithelial cells were enzymatically isolated from the cervical loop at the apical end of the lower incisors from a Sprague-Dawley rat with 1% collagenase. Dental epithelial cells were cultured with DMEM (Invitrogen) supplemented with 10% FBS for 4 weeks, then, maintained in serum-free keratinocyte synthetic medium (Keratinocyte-SFM, Invitrogen) for 1 year. An established cell line, SF2 was maintained as previously described (4). SF2 cells were transfected with a pEF6/GFP-PDGFtm-myc-HA vector expressing the GFP-PDGF receptor-transmembrane fusion protein with myc-HA tag using Lipofectamine 2000 (Invitrogen). Transfected cells were selected as SF2 subclones by culturing with media containing 400 μg/ml of G418. Twenty-five clones were selected as a stable transfected cell line, with one of them designated as SF2-24 (Ambn high expression) and another SF2-7 (Ambn low expression).

SP and MP Cell Analysis and Flow Cytometry—Hoechst staining of mDP cells for SP cell analysis was conducted as previously described (17). Subconfluent mDP cells were stained with Hoechst dye for 90 min at 37 °C. After staining, all cells were resuspended in 100 μl of Hanks' balanced salt solution (HBSS) with calcium/magnesium medium and kept on ice. The SP and MP gates were defined as previously described (17). For analysis, the cells were resuspended in ice-cold HBSS with 2% FBS containing propidium iodide (Sigma) at a final concentration of 2 μg/ml to identify dead cells, then filtered through a cell strainer. Sorting and analyses were carried out with an EPICS ALTRA flow cytometer (Beckman Coulter, Fullerton, CA). The SP cell fraction was enriched by repeating cell sorting 3 times. The expression of stem cell markers in SP cells was confirmed by flow cytometry using anti-Sca-1 and Oct3/4 antibodies (Santa Cruz Biotechnology).

Differentiation of SP Cells—For odontoblastic induction, SP cells were plated at 6×10^4 cells in 60-mm dishes. After the cells had reached 50–60% confluence, we replaced the control medium with induction medium containing 100 ng/ml of BMP2 or BMP4 (Wako Pure Chemical Industries), and cells were incubated for 2 days. For blocking BMP signaling, recombinant mouse Noggin protein (R&D systems) was

used. Total RNA was isolated and real time RT-PCR was performed using mouse Bcrp1 (18) and DSPP primer sets (supplemental Table S1).

For adipogenic differentiation, SP cells were seeded at 1×10^5 cells per well in 6-well plates and cultured in DMEM supplemented with 10% FBS. Adipogenic differentiation was induced with induction medium from a Poietics hMSC Media Bullet kit (Cambrex Bio Science Walkersville, Inc., Walkersville, MD) for 3 days and incubated in maintenance medium for 3 days, then the cells were cultured for an additional 7 days in maintenance medium. As a control, cells were cultured in only maintenance medium. Adipogenesis was confirmed by staining with Oil-Red-O and the expression of *PPARγ* was analyzed by RT-PCR.

For osteogenic differentiation, SP cells were seeded at 1.5×10^4 cells per well in 6-well plates and cultured in DMEM supplemented with 10% FBS, 10 mM β-glycerophosphate, 0.2 mM ascorbic acid, 2-phosphate, and 10^{-8} M dexamethasone. Induction and control media were replaced every 2 days. Osteogenesis was determined by alkaline phosphatase (ALP) and von Kossa staining for calcium deposition, as previously described (23). After 4 weeks culturing with osteoblast induction medium, the expressions of osteocalcin, osteonectin, and Runx2 in osteogenesis-induced SP cells were analyzed by RT-PCR.

For neurogenic differentiation, we modified a neuronal induction protocol using recombinant nerve growth factor (NGF) (Chemicon). SP cells were seeded at 1×10^5 cells per well in 6-well plates. After reaching 80–90% confluence, neurogenic differentiation was induced by culturing the cells in DMEM supplemented 2% FBS, 1.25% dimethyl sulfoxide, 10^{-6} M retinoic acid, 2.5 μg/ml insulin, and 50 ng/ml NGF. Two weeks later, neurogenesis was characterized by Western blot analysis using an anti-neurofilament-M specific antibody (Cell Signaling Technology).

Odontoblastic Induction of SP Cells by Co-culturing with Dental Epithelial Cells—We investigated the role of dental epithelial cells in specification of odontogenic cell lineage using two types of co-culture systems: feeder and chamber types with a cell culture insert (BD Falcon). We used confluent SF2 cells, or SF2 cells treated with 4% paraformaldehyde (PFA) or ammonium (denudation) as feeder cells. SF2 and SP cells were harvested and placed into either 6-well plates or cell culture inserts (chamber), then cultured until reaching confluence.

Screening of Co-culture Conditions for Ameloblastic Induction of iPS Cells—A mouse iPS cell line (iPS-MEF-Ng-20D-17), carrying the Nanog-GFP/IRES/puromycin resistant gene, was established by Yamanaka (Kyoto University, Japan), and obtained from RIKEN Cell Bank (Saitama, Japan) (6). Mouse iPS cells were cultured with rat dental epithelial cells (SF2-24), which predominantly express Ambn mRNA, as feeder cells. Preparatory co-culture experiments were performed as follows: iPS cells were cultured with mouse embryonic fibroblasts (MEFs) treated with mitomycin C (MMC) or with three different types of SF2-24 feeder cells (confluent cells, cells treated with MMC, cells treated with 4% PFA). MMC was supplied at 9 μg/ml (final concentration) for 2 h to arrest SF2-24 cell proliferation.

Induction of iPS Cell-derived Ameloblasts—iPS cells (plated $1.5 \times 10^3/cm^2$) were cultured on sheets of MMC-treated SF2-24 cells for 7, 10, and 14 days in the same medium used for the SF2-24 culture without leukemia inhibitory factor and 2-mercaptoethanol. The culture medium was changed every day throughout the co-culture period. After 7 and 10 days, the co-cultured iPS cells were subjected to RT-PCR, while those after 14 days of culture were analyzed by immunocytochemistry. Total RNA from iPS cells co-cultured with MMC-treated MEFs was isolated after 3 days of culture. Conditioned media from cultures of SF2-24 and SF2-7 were collected after 2 days of incubation. The procedures used for transfection of Ambn-expressing vectors, as well as their construction and isolation of recombinant proteins have been previously described (2, 24). K252a (Trk inhibitor, Calbiochem), PD98059 (MEK inhibitor, Cell signaling), anti-NT-4 neutralizing antibody (Applied Biological Materials), and Noggin (R&D systems) were added to conditioned medium obtained from SF2-24 cells.

Reverse Transcription-PCR—Total RNA was isolated using TRIzol (Invitrogen) and first-strand cDNA was synthesized at 50 °C for 50 min using oligo(dT) or random primers with the SuperScript III First-strand Synthesis System (Invitrogen). PCR was performed with Takara Ex Taq HotStart Version (Takara) or a PCR Additives Kit (Jena Bioscience, Germany). The primer sequences are presented in supplemental Table S1. PCR amplicons were separated and visualized on 1.5% agarose gels with SYBR Green staining using the LAS-4000 mini image analyzing system (Fujifilm). For semi-quantitative PCR analysis, the band intensities of PCR amplicons were quantified using MultiGauge software (Fujifilm) and normalized by dividing the intensity of the band of GAPDH. Because of the high degree of homology between the Ambn gene in mice and rats (94.2%), we designed a species-specific mouse Ambn primer that encoded locked nucleic acid (LNA) at a different base sequence between the mouse and rat Ambn gene in a conserved region. The specificity of the mouse Ambn primer was confirmed by PCR using mouse and rat tooth germ cDNA. Statistical analysis of gene expression was performed using the Student's *t* test.

Immunocytochemistry—For immunocytochemistry, cells were fixed with 4% PFA for 5 min at room temperature. After washing with PBS three times for 5 min, the cells were treated with Power Block Universal Reagent (BioGenex) for 5 min at room temperature, followed by three washes with PBS. The cells were incubated with the anti-Ambn primary antibody included in the kit (1:200, M-300, Santa Cruz Biotechnology). The primary antibody was visualized with Alexa Fluor 594 donkey anti-rabbit antibody (1:500, A21207, Invitrogen). Nuclei were stained with Hoechst 33258 (Invitrogen). Immunocytochemistry and phase images were captured using a BZ-8000 microscopic system (KEYENCE Co, Osaka, Japan), and images of the sections were analyzed using a BZ analyzer (KEYENCE).

RESULTS

Establishment of SP Cell Line from Mouse Dental Papilla Cells—Side population (SP) cells, which displayed stem cell ability, make up less than 1% of total cells in the mouse dental papilla (mDP) from postnatal tooth germs. Thus, biochemical and biomolecular analyses of SP cells are difficult to perform

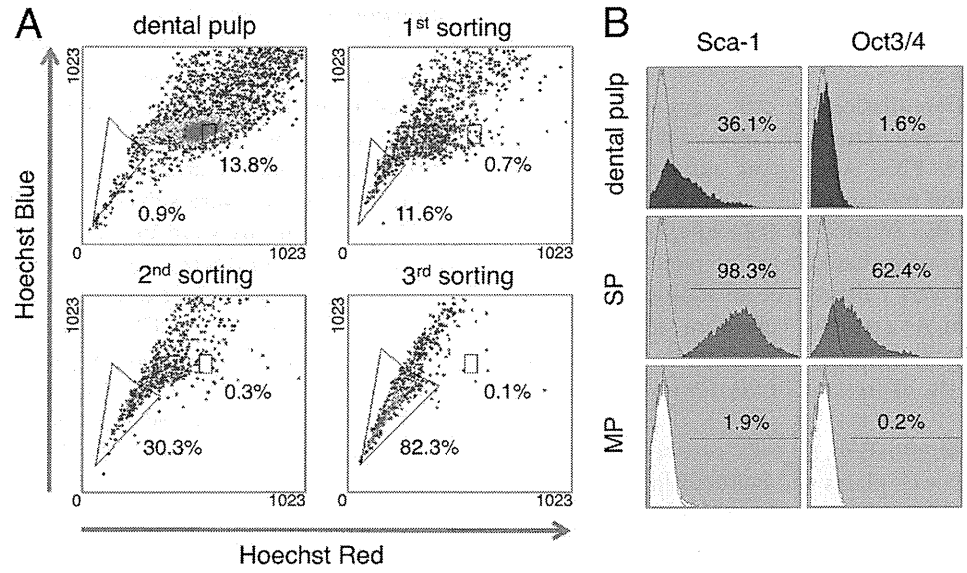

FIGURE 1. **Isolation of SP cells from mDP cell line.** *A*, flow cytometry analysis of SP cells. mDP cells made up ~0.9% of the total cell population with a relatively lower level of Hoechst 33342 fluorescence (SP cells), while 13.8% of the population was maintained as MP cells. Using repeated cell sorting, the SP cell population was enriched by 11.6% at the first sorting, 30.3% at the second sorting, and 82.3% at the third sorting. *B*, expression of the stem cell markers Sca-1 and Oct3/4 in dental pulp, SP, and MP cells.

because of the limited numbers of cells available. We enriched an SP cell population and established an SP cell line using a cell sorting technique. mDP cells were obtained from mouse incisor tooth germs and immortalized, as previously described (22). The cells were then stained with Hoechst dye and sorted to enrich the SP cell fraction. Cell sorting was repeated three times and SP cells were enriched from about 0.9% to 82.3% in the gated area (Fig. 1*A*). This SP cell line showed high expression levels of the stem cell markers Sca-1 and Oct3/4 when compared with the majority population (MP) cells, which was comprised of a greater number dental papilla cells in various differentiation stages (Fig. 1*B*).

Because the SP cells expressed a set of stem cell markers, we examined their multipotency. Using an odontoblast differentiation medium containing BMP2 or BMP4, the SP cells were induced to express DSPP, a marker of odontoblasts, whereas the expression of the undifferentiated cell marker Bcrp1 was decreased (Fig. 2*A*). In osteoblast differentiation medium, the SP cells showed increased levels of ALP and von Kossa staining, as well as expressions of the osteoblast marker genes osteocalcin, osteonectin, and Runx2, whereas the MP cells showed no induction of expression of those genes (Fig. 2, *B* and *C*). When SP cells were cultured in differentiation medium for adipogenesis or neurogenesis, they were Oil-Red-O positive or showed neurite outgrowths, along with high levels of adipogenic expression and protein expressions of neurogenic markers, such as *PPARγ* and Neurofilament-M, respectively (supplemental Fig. S1, *A--D*). These results suggest that the SP cell line established in this study has a high level of multipotency.

Expressions of Runx2 and DSPP in SP Cells Cultured with SF2 Cells—We analyzed epithelial and mesenchymal stem cell interactions by culturing SP cells with rat dental epithelial SF2 cells that had been engineered to express a GFP-myc-HA tag on the cell membrane surface. This allowed us to distinguish between SP and SF2 cell types (supplemental Fig. S2). SP cells were cultured with or without SF2 cells for 48 h, and total RNA was isolated from the mixed cell cultures (Fig. 3*A*). The expressions of Runx2 and DSPP were increased in SP cells that had been cultured with SF2 cells, as compared with those cultured without SF2 cells (Fig. 3*B*). Because Runx2 and DSPP are expressed by both odontoblasts and ameloblasts, co-cultured SP and SF2 cells were separated into individual cell populations using the anti-HA antibody, which specifically recognizes SF2 cells (Fig. 3*C*). We found a dramatic increase in the expression level of Runx2 in SF2 cells as compared with SP cells (Fig. 3*D*). No epithelial marker was detected in SP cells co-cultured with SF2 cells, suggesting that the SP cells had differentiated into odontoblasts (data not shown). Runx2 is expressed in enamel matrix-secreting ameloblasts, but not in the pre-secretion stage of ameloblasts (25). Our results suggest that the SF2 cells had fully differentiated into enamel matrix-secreting ameloblasts by co-culturing with SP cells. The expression of DSPP was up-regulated in both cell types. However, in MP cells, which are fully differentiated dental papilla cells, no expression of Runx2 or DSPP was induced by co-culturing with SF2 cells (data not shown). These results indicate that epithelial and mesenchymal stem cell interactions promote individual differential states in SF2 and SP cells.

Involvement of Exogenous Factors from Dental Epithelium in DSPP Expression of SP Cells—We attempted to identify the factors in dental epithelial cells involved in SP cell differentiation by treating SF2 cells with 4% PFA to inhibit extracellular signaling, including the effects of growth factors (Fig. 4*A*). Ammonia treatment, through a process known as denudation, removes all cell components except the extracellular matrices and is often used for three-dimensional matrix cell culture experiments (26). DSPP expression in SP cells was partially inhibited by PFA treatment, while they retained the extracellular matrix network. This result suggests that the extracellular environment including extracellular matrices, growth factors, and cell-cell

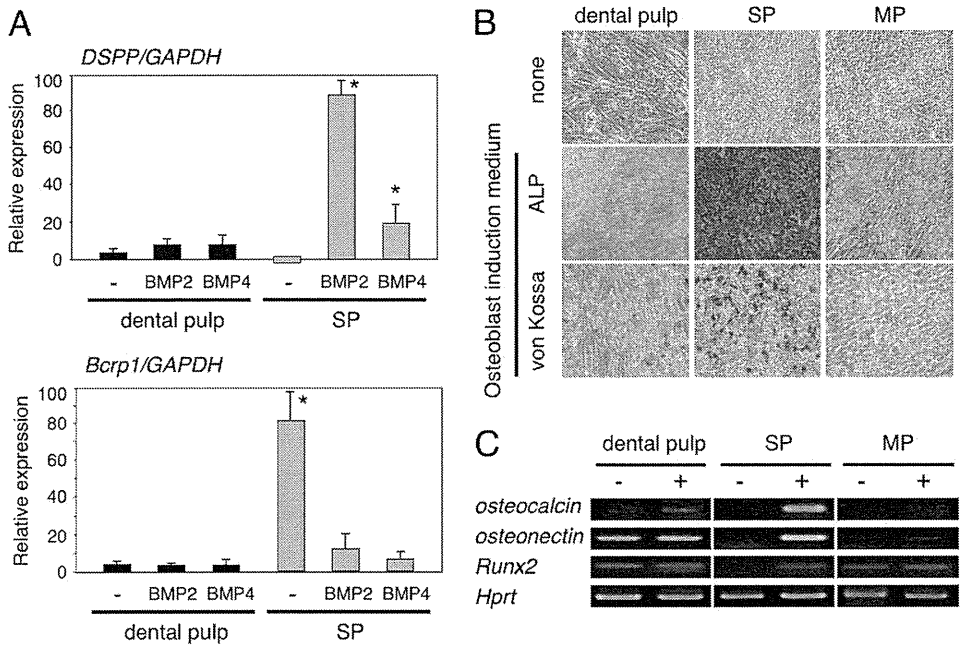

FIGURE 2. **Odontoblast and osteoblast differentiation in SP cells.** *A*, differentiation of SP cells to odontoblasts. Expression of the odontoblast marker DSPP and the undifferentiated mesenchymal marker Bcrp1 in dental pulp (*black bar*) and SP cells (*gray bar*) cultured with or without BMP2 or BMP4. *B*, differentiation of SP cells to osteoblasts in osteoblast induction medium (*Osteogenic cond.*). ALP and von Kossa staining of dental pulp, SP, and MP cells. *C*, expressions of osteoblast markers in dental pulp, SP, and MP cells cultured in regular (−) or osteoblast induction medium (+). *, $p < 0.05$.

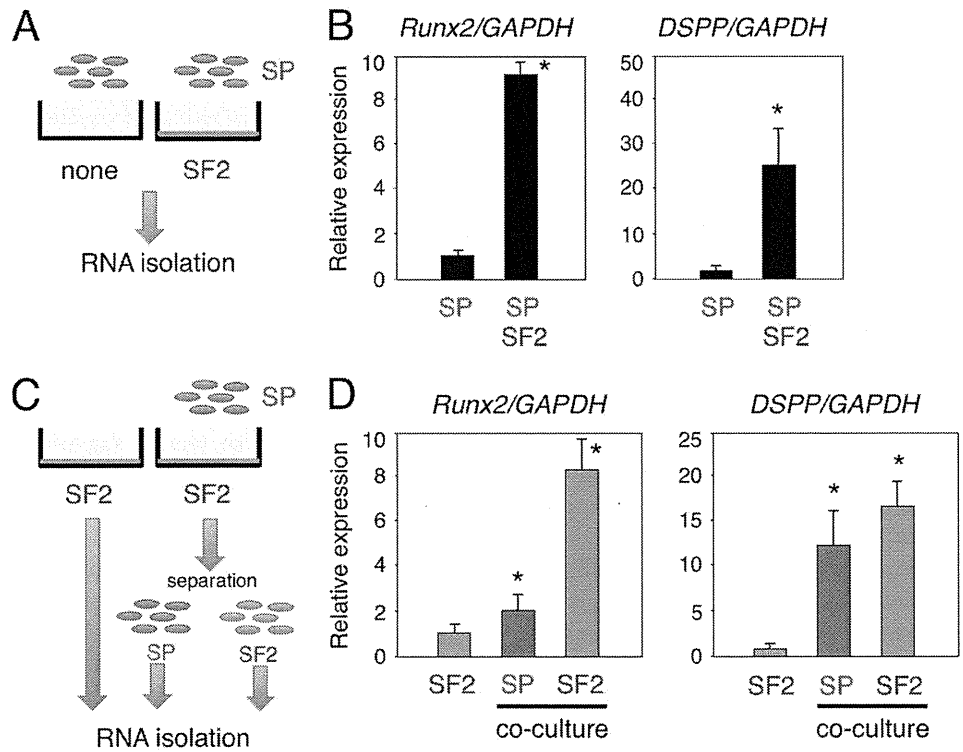

FIGURE 3. ***In vitro* epithelial-mesenchymal interaction system using dental epithelial cells (*SF2*) and dental mesenchymal stem cells (*SP*) to promote odontogenic cell differentiation.** *A* and *C*, schematic diagram of the co-culture system. *B*, comparisons of *Runx2* and *DSPP* gene expressions between the SP monolayer culture and SP and SF2 cell co-culture system. *C*, total RNA samples were separately prepared from SP and SF2 cells, using the anti-HA antibody. *D*, expressions of Runx2 and DSPP in co-cultured SF2 (*blue*) and SP (*red*) cells. The expression level of GAPDH was used an internal control. *, $p < 0.05$.

interaction produced by SF2 cells contributes to odontoblast induction. Denuded SF2 cells were also incapable of inducing DSPP expression in SP cells (Fig. 4*B*). Odontoblast induction of SP cells was observed in co-cultures with living SF2 cells, indicating that some types of soluble secreted molecules and matrices from SF2 cells are required to induce SP cells to undergo odontogenic differentiation.

Next, we screened the factors secreted from SF2 cells that promote odontogenic cell differentiation from epithelial and mesenchymal cells using cell culture chambers, which allowed

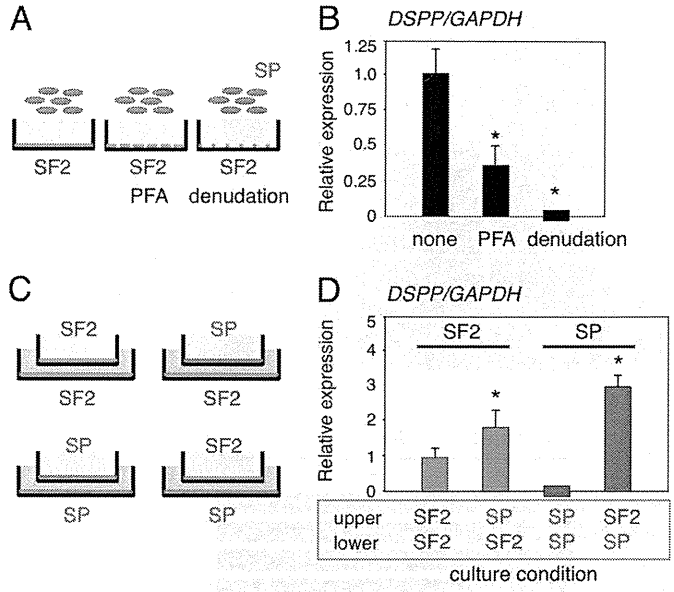

FIGURE 4. **Co-culture conditions for screening of odontogenic cell differentiation using *in vitro* cell-cell interaction system.** *A*, SP cells were cultured on SF2 cells in monolayers, then fixed with 4% paraformaldehyde (*PFA*) or treated with ammonia (denudation). *B*, DSPP expression in SP cells co-cultured under different conditions. *C*, four sets of co-culture conditions using cell chambers were analyzed. *D*, DSPP expression in SF2 cells (*blue*) and SP cells (*red*) cultured in lower dishes, with co-culture partner cells in the upper chambers. The expression level of GAPDH was used an internal control. *, $p < 0.05$.

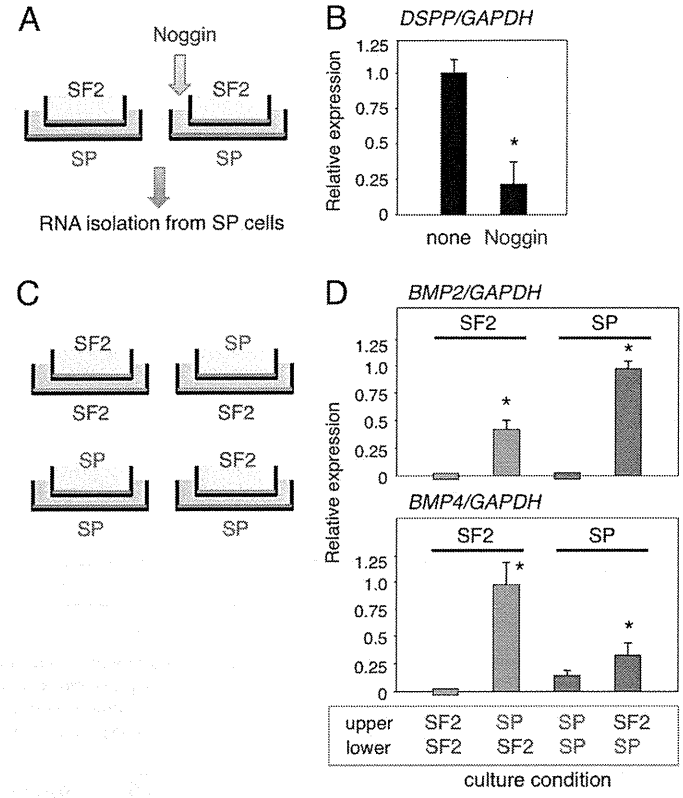

FIGURE 5. ***In vitro* epithelial-mesenchymal interaction system shows that crosstalk BMP signaling is essential for odontogenic cell differentiation.** *A*, total RNA was isolated from SP cells co-cultured with SF2 cells in the presence or absence of Noggin recombinant protein. *B*, DSPP expression in SP cells co-cultured with SF2 cells after blocking BMP signaling. *C*, four sets of culture conditions using cell chambers were analyzed. *D*, BMP2 and BMP4 expressions in SF2 (*blue*) and SP (*red*) cells, with co-culture partner cells in the upper chambers. *, $p < 0.05$.

the factors to be secreted into cell culture medium (Fig. 4*C*). Heterologous combinations of SF2 and SP cells were important for promotion of DSPP expression in both types of cells. We found that co-cultures consisting of SF2 cells in the upper chamber and SP cells in the lower chamber were most effective for stimulation of DSPP gene expression in SP cells (Fig. 4*D*). These results suggest that secreted factors are important for induction of DSPP expression in SP cells co-cultured with dental epithelial cells.

Regulation of DSPP Expression in SP Cells via BMP2-BMP4 Crosstalk—The involvement of several different types of growth factors has been reported in epithelial-mesenchymal interactions, for example, BMPs were shown to promote dental mesenchymal cell differentiation (27). We examined the potential involvement of BMPs in SP cell differentiation by adding soluble Noggin, which antagonizes BMP activity, to cell chamber cultures that contained SP cells in the lower chambers (Fig. 5*A*). The presence of Noggin in culture medium resulted in down-regulation of the expression of DSPP in SP cells as compared with the control cells (Fig. 5*B*). Therefore, BMPs are required for induction of DSPP expression in SP cells co-cultured with dental epithelial cells. In tooth germ development, BMP4 is involved in epithelial-mesenchymal interaction, and also regulates the mesenchymal expression of Msx1 and Msx2, which are important for tooth development, whereas BMP2 promotes dental mesenchymal differentiation (27). However, details regarding crosstalk between BMP2 and BMP4 in dental epithelial and mesenchymal stem cell interactions have not been elucidated. We sought to clarify the role of BMPs in these interactions by examining the expressions of BMP2 and BMP4 in SF2 and SP cells using a separated chamber assay (Fig. 5*C*). The expression of BMP2 was higher in SP cells than SF2 cells under the heterologous combination culture condition, whereas BMP2 was not detected in homologous cultures (Fig. 5*D*). In contrast, the expression of BMP4 was higher in SF2 cells than in SP cells in the heterologous combinations (Fig. 5*D*). Taken together, these results suggest that the interactions between dental epithelium and dental mesenchymal stem cells induce BMP4 and BMP2, which, in turn, promote odontogenic cell differentiation via paracrine and autocrine signaling.

Optimization of Co-culture Conditions for Differentiation of iPS Cells into Ambn-expressing Dental Epithelial Cells—Following interaction with SF2 cells, SP cells differentiated into DSPP expressing cells, but not ameloblasts (Figs. 3, 4, and 5). This may be because SP cells are mesenchymal stem cells and committed to differentiate into mesenchyme lineage cell types. Therefore, we used mouse iPS cells to examine whether these cells can be differentiated into ameloblasts when cultured with SF2 cells. However, SF2 cells did not effectively promote their differentiation (data not shown), which may be due to the necessity of factors from differentiated dental epithelial cells for differentiation of iPS cells into ameloblasts. To test this possibility, we subcloned 25 different SF2 cell lines and examined the expression levels of the Ambn gene. Of these lines, the SF2-24 cell line expressed Ambn at the highest level (supplemental Fig. S3*A*). Dental epithelium SF2-24 cells grew tightly together in a

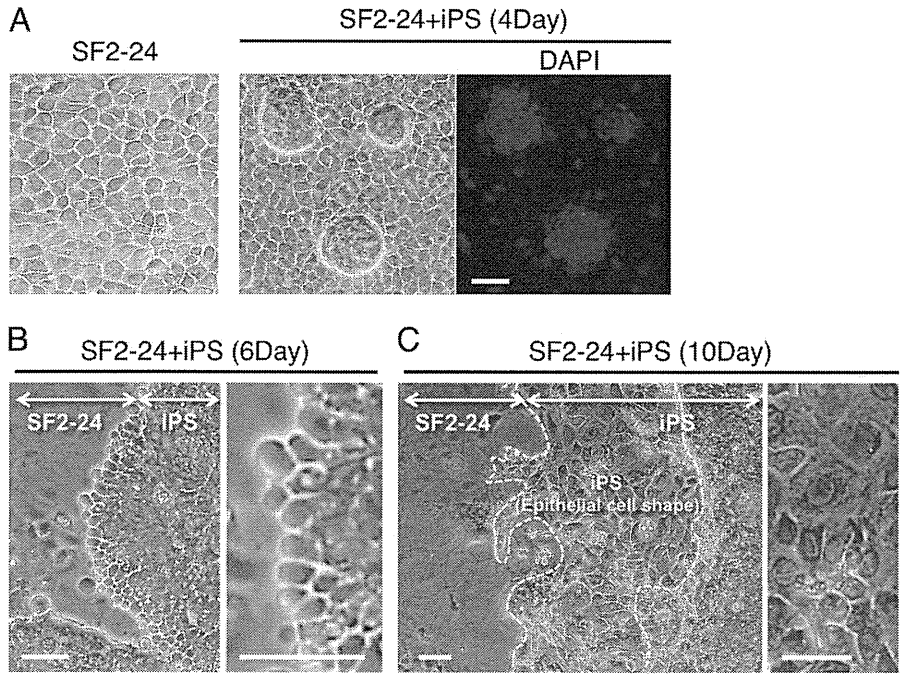

FIGURE 6. **Epithelial cell shapes of iPS cells after co-culturing with SF2-24 cells.** *A*, phase micrographs of monolayer SF2-24 cells and iPS cells cultured with SF2-24 feeder cells for 4 days, followed by DAPI staining. *B* and *C*, low and high magnification phase micrographs of iPS cells on MMC-treated SF2-24 feeder cells after 6 (*6Day*) and 10 days (*10Day*). Enlarged image shows a part of the iPS cells with epithelial cell shapes. *C*, epithelial cell cluster formed by iPS cell-derived epithelial cells (area within *yellow dashed line*). Bar, 50 mm.

square or cuboidal shape (Fig. 6*A*), and expressed Ambn and cytokeratin-14 (CK14), but not the reprogrammed factors Sox2, Klf4, and Oct3/4 (supplemental Fig. S3*B*). On the other hand, iPS cells formed colonies that expressed Nanog promoter-driven GFP (data not shown) as well as Klf4, Sox2, Oct3/4, and Nanog, but not Ambn or CK14 (supplemental Fig. S3*B*).

We also examined the effects of differentiation by co-culturing iPS cells with MMC-treated non-proliferating SF2-24 feeder cells (Fig. 6*A*). The shape of the co-cultured iPS cells was clearly rounded along the boundary of the clusters after 6 days (Fig. 6*B*). These cells had migrated and formed what appeared to be epithelium after 10 days (area surrounded by *yellow dashed line*, Fig. 6*C*).

The differentiation of iPS cells was then determined by RT-PCR analysis. First, we examined the specificity of mouse Ambn locked nucleic acid (LNA) primer sets (supplemental Fig. S4). A mouse Ambn LNA primer set specifically detected the mouse Ambn gene, but not the rat Ambn gene (supplemental Fig. S4*A*). Using this primer set, Ambn expression was not detected in mouse iPS cells or MEFs (supplemental Fig. S4*B*). Next, we examined co-culture conditions for the differentiation of iPS cells into dental epithelium (Fig. 7*A*). iPS cells co-cultured with MMC-treated SF2-24 cells showed a high expression of the mouse Ambn gene, while those co-cultured with PFA-treated or non-treated SF2-24 cells did not (Fig. 7*B*). SF2-24 feeder cells expressed rat Ambn when co-cultured with iPS cells, while that expression was reduced at 10 days (Fig. 7*C*).

Interestingly, expressions of the stem cell markers Sox2, Oct3/4, Nanog, Fgf4, and Gdf3 were not changed throughout the co-culture period, because of the existence of undifferentiated iPS cells (Fig. 7*C*), while those of the endodermal markers Cdx2 and Gata6 were also not increased. Furthermore, the mesodermal marker Brachyury was highly expressed in iPS cells, because of technical contamination resulting RNA extraction from MEFs used for maintenance of the iPS cells, and then gradually decreased over time. We also observed increased expressions of the mouse ameloblast markers Ambn and Enamelin (Enam), as well as the epithelial markers CK14 and p63, in iPS cells after 7 and 10 days (Fig. 7*C*). Furthermore, the expression of epiprofin/Sp6, a transcription factor highly expressed in dental epithelium (28), was increased in those cells (supplemental Fig. S5). A similar expression pattern was observed in co-cultured iPS cells separated from SF2-24 cells using the anti-HA antibody (data not shown).

Differentiation of iPS Cells into Ambn-expressing Dental Epithelial Cells—We then examined the protein expression of Ambn in iPS cells using immunostaining. Approximately 95% of the epithelial-like cells were positive for Ambn (Fig. 8*A*), while the immunofluorescence intensity of Ambn was stronger in iPS cells than in SF2-24 cells (Fig. 8*B*). Therefore, mouse iPS cells differentiated into dental epithelium, but not into endodermal or mesodermal cells.

We attempted to identify the factors involved in differentiation of iPS cells into dental epithelium by culturing with MEFs in medium conditioned by SF2-24 cell cultures (Fig. 9*A*). Culturing with SF2-24 condition medium induced the expression of Ambn in iPS cells, indicating an involvement of soluble factors including growth factors, and extracellular matrices derived from SF2-24 cells (Fig. 9*B*). Next, we examined the effect of Ambn on differentiation of iPS cells into dental epithelial cells. Expression vectors for the full-length (AB1), C-terminal (AB2), and N-terminal (AB3) half of Ambn (Fig. 9*C*) were separately transfected into Ambn low-expressing cells (SF2-7), then conditioned media from those cells or recombinant Ambn